

# iShocks: X-ray binary jets with an internal shocks model

O. Jamil<sup>1</sup>\*, R. P. Fender<sup>1</sup> and C. R. Kaiser

<sup>1</sup>University of Southampton, U.K.

Accepted 03 September 2009

## ABSTRACT

In the following paper we present an internal shocks model, iShocks, for simulating a variety of relativistic jet scenarios; these scenarios can range from a single ejection event to an almost continuous jet, and are highly user configurable. Although the primary focus in the following paper is black hole X-ray binary jets, the model is scale and source independent and could be used for supermassive black holes in active galactic nuclei or other flows such as jets from neutron stars. Discrete packets of plasma (or ‘shells’) are used to simulate the jet volume. A two-shell collision gives rise to an internal shock, which acts as an electron re-energization mechanism. Using a pseudo-random distribution of the shell properties, the results show how for the first time it is possible to reproduce a flat/inverted spectrum (associated with compact radio jets) in a conical jet whilst taking the adiabatic energy losses into account. Previous models have shown that electron re-acceleration is essential in order to obtain a flat spectrum from an adiabatic conical jet: multiple internal shocks prove to be efficient in providing this re-energization. We also show how the high frequency turnover/break in the spectrum is correlated with the jet power,  $\nu_b \propto L_W^{\sim 0.6}$ , and the flat-spectrum synchrotron flux is correlated with the total jet power,  $F_\nu \propto L_W^{\sim 1.4}$ . Both the correlations are in agreement with previous analytical predictions.

**Key words:** X-Ray binaries, jets, internal shocks, adiabatic losses, synchrotron spectrum, infra-red, radio, flat/inverted spectrum

## 1 INTRODUCTION

In recent years there has been a lot of interest in probing the disc-jet connection in a variety of astrophysical objects. The mechanisms behind the jet formation are still not fully understood, leaving many open questions: the origin of a flat spectrum ( $\alpha \sim 0$  when  $F_\nu \propto \nu^\alpha$ ) is one such question. The flat spectra have been observed both in active galactic nuclei (AGN) (for a review see Cawthorne 1991) and X-ray binaries (XRBs) (Fender 2001); in the XRBs it has been seen to extend from Radio to near infra-red (Corbel & Fender 2002). It is thought that this spectrum originates from the jet via the partially self absorbed synchrotron emission.

The Blandford & Königl (1979) model attempts to explain how such a flat spectrum could arise. In their model, the jet is assumed to be conical with the magnetic field perpendicular to the jet axis and frozen in plasma. For a given frequency, an increase in the jet volume causes a decrease in the plasma optical depth. The inner, denser, parts of jets are optically thick to lower frequencies (e.g. radio): the higher the energy density of the jet volume, the higher the optical depth (for a given frequency). The radio frequencies

therefore peak in the outer parts of the jet, while the infra-red peak in the inner parts of the jet. The one drawback of the Blandford & Königl (1979) model is the artificial replenishment of the adiabatic energy losses suffered by the jet plasma. Marscher (1980) showed a model that takes electron energy losses into account, but are unable to reproduce a flat spectrum; Hjellming & Johnston (1988) presented a model where it is possible to obtain a flat spectrum under slowed expansion for a conical jet. A comprehensive study by Kaiser (2006) (more recently Pe’er & Casella 2009) shows that if the adiabatic losses are not replenished then it is impossible to obtain a flat spectrum from a conical jet. Kaiser (2006) also show that using a non-conical jet volume, it is possible to recover a flat spectrum even with energy losses: the jet geometry requires fine tuning to minimize the adiabatic losses normally associated with a conical jet, while allowing enough of a change in volume to drive the changes in optical depth.

In the following paper, we present a model that addresses the problem of electron re-energization via a large number of ‘small’ shell collisions. Although the main focus in this paper is on black hole XRB jets, the model is not restricted to such systems: the model is scale independent and AGN jet volumes can also be simulated. The first part of the

\* E-mail: oj1@soton.ac.uk

paper goes through the details of the model, outlining the physics and the techniques employed. The results section is split into different jet scenarios: single ejection, double ejection (single collision/internal shock), and multiple ejections (multiple internal shocks). The results from these increasingly complex scenarios are used to demonstrate the model's capabilities, in addition to exploring the internal physics of the relativistic jets.

## 2 THE MODEL

Our model is based on the Spada et al. (2001) internal shocks model for radio-loud quasar. Many modifications, however, have been carried out to make the model more flexible, and applicable to different scales and scenarios. In our model the jet is simulated using discrete packets of plasma or *shells*. For simplicity, only the jets at relatively large angle of sight are treated. Each shell represents the smallest emitting region and the resolution in the model is limited to the shell size. While the simulation is running, the jet can 'grow' with the addition of shells at the base as the previously added shells move further down the jet. If the time interval between consecutive shell injections is kept small, a continuous-jet approximation is achieved. The variations in shell injection time gap and velocity cause faster shells to catch up with slower ones, leading to collisions: the internal shocks, discussed later, are a result of shell collisions. A schematic of the model set up is shown in figure 1: the two conical frusta shown represent the shells.

### 2.1 Shell properties

The shell volume is based on a conical frustum (cone opening angle = jet opening angle,  $\varphi$ ). As a shell moves down the jet, it can expand laterally as well as longitudinally (figure 1). The adiabatic energy losses are a result of the work done by a shell in expanding; implicit assumptions are made about the pressure gradient across the jet boundary that would result in a conical jet. The emitting electron distribution is assumed to be power-law in nature; each shell contains its own distribution. The power-law distribution is of the form:

$$N(E)dE = \kappa E^{-p} dE, \quad (1)$$

where  $E = \gamma mc^2$  is the electron energy,  $p$  is the power-law index and  $\kappa$  is the normalization factor. If the total kinetic energy density of the electrons,  $E_k$ , is known then  $\kappa$  can be calculated for the two cases of power-law index:  $p \neq 2$ , and  $p = 2$ . When  $p \neq 2$ , we have (with the electron energy is expressed in terms of the Lorentz factor with  $mc^2 = 1$ ):

$$E_k = \kappa \left[ \frac{1}{(2-p)} (\gamma_{max}^{(2-p)} - \gamma_{min}^{(2-p)}) - \frac{1}{(1-p)} (\gamma_{max}^{(1-p)} - \gamma_{min}^{(1-p)}) \right], \quad (2)$$

and for  $p = 2$ :

$$E_k = \kappa \{ [\ln(\gamma_{max}) - \ln(\gamma_{min})] + [\gamma_{max}^{-1} - \gamma_{min}^{-1}] \}, \quad (3)$$

where the subscripts *max* and *min* denote the upper and lower energy bounds for the electron distribution. The relations given in equations 2 and 3 can therefore be used

to calculate the change in electron power-law distribution when there is a change in the total kinetic energy density, assuming the power-law index and  $\gamma_{min}$  are fixed.  $\gamma_{min}$  value throughout the following work is set equal to unity, while the power-law index is assumed to be 2.1. The electron energy distribution upper limit,  $\gamma_{max}$ , is initially set to be  $10^6$ , but allowed to vary with the energy losses.

A magnetic field is essential to give rise to the synchrotron radiation. In the shells, the magnetic field is assumed to be constantly tangled in the plasma, leading to an assumption that the magnetic field is isotropic; hence, treated like an ultra-relativistic gas (Heinz & Begelman 2000). If the magnetic energy density ( $E_B$ ) is given, the field ( $B$ ) can be calculated:

$$E_B = \frac{B^2}{2\mu_0}, \quad (4)$$

where  $\mu_0$  is the magnetic permeability.

Other shell properties include the bulk Lorentz factor,  $\Gamma$ , and the shell mass,  $M$ . If there is a variation in the  $\Gamma$  of different shells in the jet, then the faster inner shells are able to catch up with the slower outer ones, causing shell collisions; the shell collisions create internal shocks, which ultimately generate the internal energy.

### 2.2 Internal shocks

When two shells collide, a shock forms at the contact surface. Some of the steps involved in two-shell collision, and the subsequent merger, are shown in figure 2. The collision are considered to be inelastic. With many shells present inside the jet, first we need to calculate the next collision time between two shells: a collision is said to occur when the outer boundary of the inner shell,  $R_j^{outer}$ , comes in contact with the inner boundary of the outer shell,  $R_{j-1}^{inner}$ . The following relation can be used to calculate the time interval for two shell collision:

$$dt_{coll} = \frac{R_{(j-1)}^{inner} - R_{(j)}^{outer}}{(\beta_{(j-1)}^e + \beta_{(j)}^e)c + (\beta_{(j)} - \beta_{(j-1)})c}, \quad (5)$$

where the subscripts  $j-1, j$  denote two consecutive shells,  $\beta_e$  is the shell longitudinal expansion velocity (along the jet axis), and  $\beta$  is the shell velocity ( $= \sqrt{\Gamma^2 - 1}/\Gamma$ );  $dt$  is calculated for all the shells inside the jet and the minimum of these collision time gaps is selected i.e. the next earliest collision. The shell longitudinal expansion ( $\beta_e$ ) is due to any thermal energy the shell may have. We do not explicitly model a thermal electron population; however, the expansion effects of having such a population are incorporated in the model. The shell expansion velocity is given by (Spada et al. 2001):

$$\beta_e = \frac{2\beta'_s}{\Gamma^2} \frac{1}{1 - (\beta\beta'_s)^2}, \quad (6)$$

where  $\beta_s = v'_s/c$  corresponds to the sound velocity in the plasma (in shell co-moving frame), and:

$$v'_s = \sqrt{\frac{1}{3} \frac{E'_{th}}{M}}, \quad (7)$$

with  $E'_{th}$  being the shell thermal energy and  $M$  is the shell mass. The prime denotes quantities in the shell rest frame.

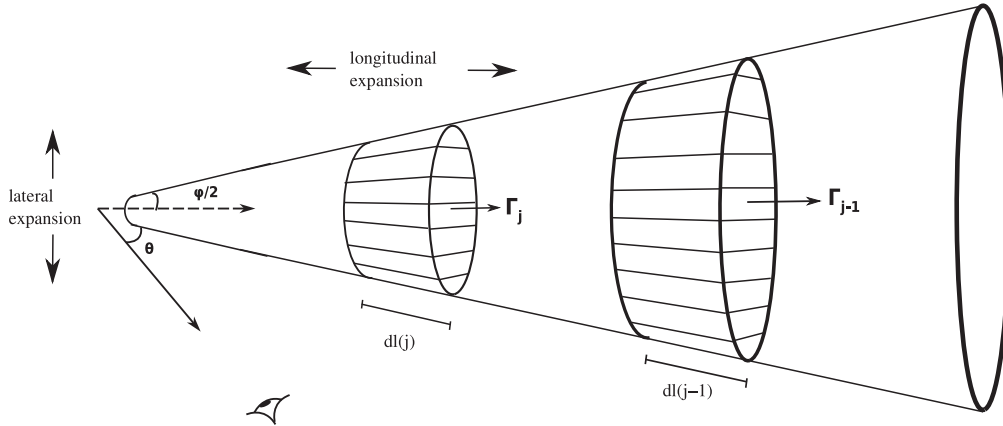


**Figure 1.** An illustration of shells in our jet model. If the outer boundary of the inner shell, ( $j$ ), contacts the inner boundary of the outer shell, ( $j-1$ ), a collision is said to occur. The lateral expansion is due to jet opening angle; the longitudinal expansion is due to the shell walls expanding within the jet. The illustration is not to scale.

The Panaitescu & Mészáros (1999) treatment of shock propagation is followed to work out the various quantities associated with the shock itself. The shock propagation can be split into two shock-fronts. The forward shock traveling from the contact surface and through the outer shell ( $j-1$ ). The reverse shock travels through the inner shell ( $j$ ) (injected after shell ( $j-1$ )). Once the shock-front has passed through, the plasma/shell is considered to be *shocked* (S) and will have different physical properties compared to the unshocked plasma (see figure 2). In one of the shell co-moving frames (shell rest-frame), the shock-front (SF) velocity can be calculated as:

$$\beta'_{SF} = \frac{(\Gamma'_S - 1)(\hat{\gamma}\Gamma'_S + 1)}{\beta'\Gamma'_S[\hat{\gamma}(\Gamma'_S - 1) + 1]}, \quad (8)$$

$\hat{\gamma}$  is the adiabatic index and  $\Gamma'_S$  corresponds to the shocked plasma and is given by:

$$\Gamma'_S = \Gamma_m \Gamma (1 - \beta_m \beta), \quad (9)$$

where the subscript  $m$  denotes the merged shell properties. The merged shell is formed once the shock-fronts have passed through both shells, leaving one combined shell. The merged shell mass is simply the linear combination of the two merging shells i.e.

$$M_m = M_{(j)} + M_{(j-1)}, \quad (10)$$

while the merged shell Lorentz factor is given by (Spada et al. 2001):

$$\Gamma_m = \left( \frac{\mu_{(j)}\Gamma_{(j)} + \mu_{(j-1)}\Gamma_{(j-1)}}{\mu_{(j)}/\Gamma_{(j)} + \mu_{(j-1)}/\Gamma_{(j-1)}} \right)^{1/2}, \quad (11)$$

where  $\mu = M + \eta/c^2$  and  $\eta$  is the shell internal energy. As the shell collisions are considered inelastic, the generated internal energy is given by:

$$E_{in} = \eta_{(j)} + \eta_{(j-1)} + \mu_{(j)}c^2(\Gamma_{(j)} - \Gamma_m) + \mu_{(j-1)}c^2(\Gamma_{(j-1)} - \Gamma_m). \quad (12)$$

Once the quantities, outlined above, associated with the shocked plasma are calculated, we are able to determine the new merged shell length. Due to the shock prop-

agation through the plasma, the two shell lengths cannot be combined linearly to give the merged shell length. The shock propagation has a compression effect on the shell; the merged shell length is given by:

$$dl_m = \frac{dl_{(j)}}{\rho_{(j)}} + \frac{dl_{(j-1)}}{\rho_{(j-1)}}, \quad (13)$$

and the density,  $\rho$ , is:

$$\rho = \frac{\Gamma_m \hat{\gamma} \Gamma'_S + 1}{\Gamma \hat{\gamma} - 1}. \quad (14)$$

The Lorentz factor,  $\Gamma$ , corresponds to one of the two shells involved in the collision while  $\Gamma'_S$  is given by equation 9. We do not consider the re-energization of the new merged shell to be instantaneous, but instead the energy is dissipated over a time period the shock-fronts would take to cross the inner and outer shells combined i.e.

$$dt_{ER} = \frac{dl_{(j)}}{\beta_{RS}} + \frac{dl_{(j-1)}}{\beta_{FS}}, \quad (15)$$

where the subscripts  $ER$ ,  $FS$  and  $RS$  denote energy release (time), forward shock and reverse shock respectively. Due to the limitations in the way the shocks are modelled, the merged shell is given the corresponding length (equation 13) at the point of creation; only the energy release is delayed over time  $dt_{ER}$ . If the adiabatic energy losses are taken into account, then the merged shell will also be losing energy during the period  $dt_{ER}$ .

### 2.3 Adiabatic losses

For an expanding conical jet, the adiabatic energy losses need to be taken into account. These energy losses are due to the work done by the jet material while expanding ( $dU = -PdV$ , where  $U$ ,  $P$  and  $V$  are energy, pressure and volume respectively). Using the relation,  $P = nkT$ , and assuming that all the synchrotron emitting electrons are highly relativistic, we have:

$$\frac{\gamma}{\gamma_0} = \left( \frac{V}{V_0} \right)^{-\frac{1}{\gamma}}, \quad (16)$$

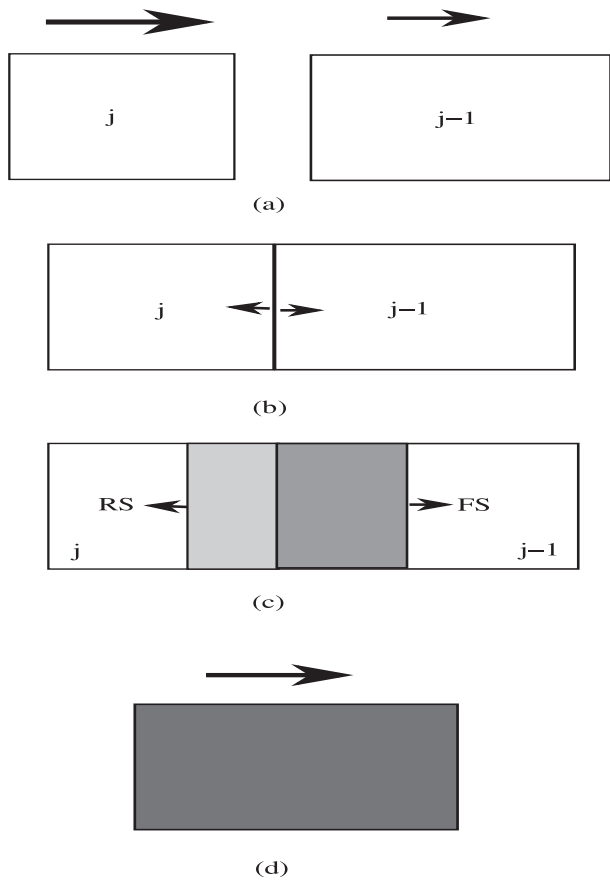


**Figure 2.** An illustration of a two shell collision leading to a merger: (a) when the inner shell,  $j$ , comes in contact with the outer shell,  $j-1$ , (b) a shock starts to form; (c) the forward shock, FS, travels through the outer shell while the reverse shock, RS, travels through the inner shell; (d) once shock fronts have traversed the two shells, a new ‘merged’ shell is formed.

with the adiabatic index,  $\hat{\gamma} = 3$ ; the subscripts ‘0’ denote quantities before the change in volume; the Lorentz factor  $\gamma$  corresponds to the power-law electrons accelerated to high energies due to the shock-front passing through the plasma. The adiabatic energy losses for the kinetic energy contained in the power-law electron distribution can therefore be calculated using equation 16. To calculate the change in the power-law normalization,  $\kappa$ , for a change in volume, the following relation is used:

$$\kappa = \kappa_0 \left( \frac{V}{V_0} \right)^{\frac{-p-2}{3}}. \quad (17)$$

Once the power-law normalization is, initially, calculated using equation 2 or 3, the above relation can then be used to calculate the subsequent changes in the normalization. If the shell is involved in another collision then the distribution is re-calculated completely. The change in the maximum Lorentz factor of the electrons,  $\gamma_{max}$ , as the shell volume changes, can be calculated using equation 16. The combined effect of varying  $\gamma_{max}$  and  $\kappa$  is to effectively ‘evolve’ the power-law electron distribution.

The changes in the magnetic energy density can be determined in a similar manner. If we assume that the magnetic field is constantly entangled in the plasma and treat it

as an ultra-relativistic gas, we can calculate the changes in magnetic pressure,  $P(B)$  using:

$$PV^{\hat{\gamma}} = P_0V_0^{\hat{\gamma}}, \quad (18)$$

therefore,

$$P(B) = P_0(B) \left( \frac{V}{V_0} \right)^{-\frac{1}{\hat{\gamma}}}, \quad (19)$$

where the adiabatic index  $\hat{\gamma} = 4/3$ .

## 2.4 Partially self absorbed synchrotron emission

To model the synchrotron radiation, we employ the treatment outlined in Longair (1994). With only the power-law electrons present, the synchrotron emission calculation is simplified; the synchrotron monochromatic intensity is given by:

$$I_\nu = \delta_{\mp}^3 \frac{J_\nu}{4\pi\chi_\nu} (1 - e^{-\chi_\nu r}). \quad (20)$$

The emission coefficient,  $J_\nu$ , and the absorption coefficient,  $\chi_\nu$ , are given by Longair (1994). These coefficients are a function of the power-law normalization and the magnetic field, which in turn depends on the energy density of the shells;  $r$  is the shell radius ( $\tau_\nu = \chi_\nu r$ ); the Doppler factor,  $\delta_{\mp}$ , is:

$$\delta_{\mp} = [\Gamma(1 \mp \beta(\cos\theta))]^{-1}, \quad (21)$$

where,  $\theta$  is the jet viewing angle and ‘ $\mp$ ’ corresponds to either an approaching component or a receding component of the jet.

If the shell area is given by  $A$  and the distance to the jet is  $D$ , then the flux,  $dF_\nu$ , from a single shell has the following form:

$$dF_\nu = \delta_{\mp}^3 \frac{A}{4\pi^2 D^2} \frac{J_\nu}{\chi_\nu} (1 - e^{-\chi_\nu r}). \quad (22)$$

The above relations are used to self consistently calculate the synchrotron spectrum as it varies with the shell properties. A more indepth treatment of the radiative transfer should take the relativistic effects, such as the relativistic aberration, into account as they may affect the overall spectral normalization. However, with simplicity in mind, these effects are not taken into account here: any errors due to this approximation can be minimized by only treating the jets at a large angle of sight.

When a shell expands, its optical depth (with respect to a given frequency) changes; hence, a shell that is optically thick to radio frequencies can become optically thin to them, as it moves down the jet. The optical depth of the neighbouring shells is not taken into account when calculating the emission from a given shell; only the jets at relatively large angle sight from the viewer can be modelled. In other words, only the emission directly from each individual shell is modelled.

## 2.5 Model parameters

So far, only some of the physics and the principles behind the model have been outlined. It is therefore important to list some of the parameters used in our model to see how

they influence the physical properties of a jet (appendix A contains all the model parameters).

The internal energy of the shell is split between the electron kinetic energy ( $u_e$ ), shell thermal energy ( $u_{th}$ ) and magnetic energy ( $u_B$ ) i.e.

$$E_{int} = u_e + u_{th} + u_B . \quad (23)$$

Equipartition between the electron kinetic and magnetic energy is assumed. The thermal energy density,  $u_{th}$ , is assumed to be solely responsible for the longitudinal expansion of the shells. Although the power-law electrons would also exert pressure for a similar effect, this becomes more important when  $u_{th}$  is zero. However, any *realistic* jet scenario is modelled with the thermal population present; the zero-thermal-energy scenario is used mainly for demonstrative purposes. Also if the shell mergers are not taking place and all the injected shells are identical, the longitudinal expansion needs to be suppressed, otherwise equation 11 generates an erroneous value for the merged  $\Gamma_m$ . Of course, a more detailed treatment for any future work, take into account not only the power-law electron pressure, but also model the synchrotron emission from the thermal population.

It maybe possible to constrain the distance to the source ( $D$ ) and the jet viewing angle ( $\theta$ ) from observations. The shell mass on the other hand offers a free parameter. In case of massive ejection event, the mass can be set manually. For a continuous jet (multiple ejections), we have a choice of setting the individual shells' properties manually or sampling from a *pseudo*-random distribution of these parameters. In the *pseudo*-random case, if the jet kinetic luminosity,  $L_W$ , is known then it can be used to generate the shell mass values by using:

$$\sum_{j=1}^N M_j \Gamma_j c^2 = L_W t_{jet} , \quad (24)$$

where  $t_{jet}$  is the duration the jet is “on”. Therefore the total relativistic mass of all the shells present in the jet has to correspond to the jet kinetic luminosity of the jet being modelled. The time gap,  $d_{inj}$ , between any two shells can also be set either manually or sampled from a Gaussian distribution with a given mean and standard deviation. The shell bulk Lorentz factor ( $\Gamma$ ), if not set manually, is picked from a random distribution of values with the maximum and the minimum values ( $\Gamma_{max}, \Gamma_{min}$ ) set by the user; the bulk Lorentz factor for a shell does not vary as it moves through the jet, unless it is involved in a collision. The shell length ( $dl$ ) and the jet opening angle ( $\varphi$ ) are not constrainable from observations. However, at least in the case of the shell length, attempting to achieve a continuous jet approximation results in the following relation:

$$dl = l_{scale} dt_{inj} \beta_{shell} c , \quad (25)$$

where  $l_{scale}$  is a scaling factor with a maximum of unity.  $l_{scale} = 1$  means no spatial gap between two consecutively injected shells; in the simulation, however,  $l_{scale} < 1$  in order to avoid a ‘pile-up’ of shells at the source.

### 3 RESULTS

With the aim of demonstrating a few of our model’s capabilities, the following section is split into three main scenar-

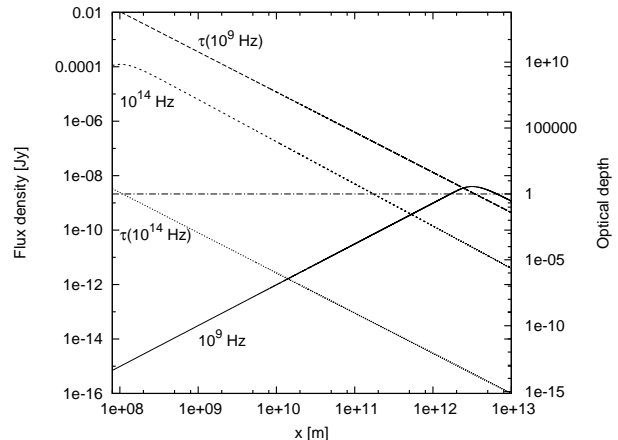


**Figure 3.** Emission from a single shell: radio and infra-red frequencies are shown. The shell optical depth,  $\tau_\nu$ , is also shown; the horizontal line marks optical depth of unity.

ios: single ejection, double ejection, and multiple ejections. Within each scenario, the effects of adiabatic energy losses are also explored. As stated earlier, the focus in the following sections is on black hole XRB jets; accordingly various shell properties, outlined above, are calculated and estimated for XRB scaled jets.

#### 3.1 Single ejection

A single shell ejection scenario can be used to simulate the massive ejection events observed in X-ray binaries, in the form of radio flares, when the source is transitioning from a hard state to a soft state (Fender et al. 2004). When shells are injected into the jet, they only start emitting radiation, or “light-up”, when they have been involved in a collision i.e. the shock front has passed through and energized the plasma within the shell (unless if they are injected with internal energy). In the case of a single shell, however, no collisions can take place; thus, the shell will require lighting-up artificially. This is achieved by creating a “shock-zone” at an arbitrary point,  $x_{shock}$ , along the jet; the *shock-zone* picture is reminiscent of the jet models involving a single-shock-zone in the jet (see Falcke 1996, Falcke & Markoff 2000, Markoff et al. 2001, Markoff et al. 2003, Pe’er & Casella 2009 and the references therein). In our model, once a shell passes through the shock zone it is energized instantly. A fraction of the shell’s relativistic energy,  $E_{frac}$ , is used as a scaling for the amount of internal energy given to a shell after energization; the shell velocity,  $\Gamma$ , and mass,  $M$ , remain unchanged.

##### 3.1.1 Without energy losses

Not taking the shell energy losses, as it expands, into account is similar to assuming that any energy losses are continually replenished (Blandford & Königl 1979). With this kind of set up, a shell is allowed to propagate down the jet and expand laterally. The shell longitudinal expansion, due to the thermal energy of the plasma, is suppressed: the thermal energy is set to zero. The change in volume is therefore not associated with any work done by the shell.

The emission at radio and infra-red frequencies, from a

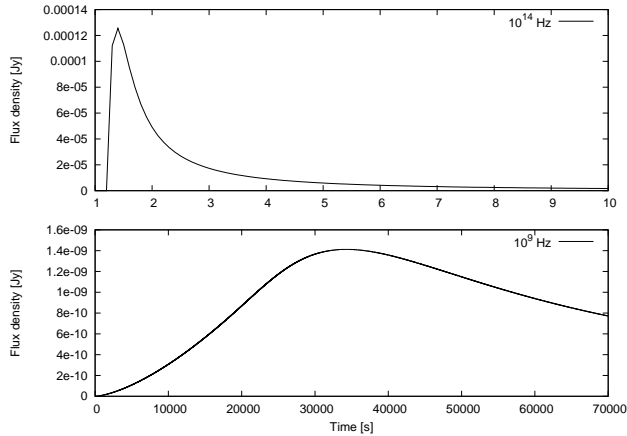


**Figure 4.** Infra-red and radio lightcurves for a single shell without adiabatic energy losses.

**Table 1.** The parameters used for single ejection scenarios.

Parameter	fig 3, 4	fig 5, 6
$\varphi$	$5^\circ$	$5^\circ$
$\theta$	$40^\circ$	$40^\circ$
$D$	2 kpc	2 kpc
$M$	$1 \times 10^7$ kg	$1 \times 10^7$ kg
$\Gamma$	2.0	2.0
$dl$	$1 \times 10^4$ m	$1 \times 10^4$ m
$u_e$	0.5	0.5
$u_B$	0.5	0.5
$u_{th}$	0.0	0.0
$x_{shock}$	0.2 ls	0.2 ls
$E_{frac}$	0.3	0.3
Sim. Duration	$7 \times 10^4$ s	500 s

single shell, is shown in figure 3. The plot also shows how the shell optical depth for the two frequencies changes as the shell moves down the jet. The increase in shell volume causes the shell to become optically thinner to lower frequencies. This behaviour is evident in the figure, as the radio emission peak is much further down the jet than the infra-red peak: the emission peaks at  $\tau_\nu \approx 1$ . Various shell and jet volume parameters are outlined in table 1.

The radio and the infra-red lightcurves, in figure 4, illustrate how the radio rise time is much longer than that of the infra-red. These rise times are determined by the shell energy density, and how quickly this energy density changes with the change in volume. Therefore, in the case shown here, the shell properties are such that the infra-red peaks rapidly after the injection, but the radio takes much longer. It should be noted that because energy losses are not considered here, only the energy density of the shell, due to lateral expansion, is decreasing; the shell's total energy content remains fixed.

### 3.1.2 With adiabatic energy losses

When the adiabatic energy losses are taken into account, an increase in shell volume causes a decrease in the shell internal energy. In this particular simulation, as in the pre-

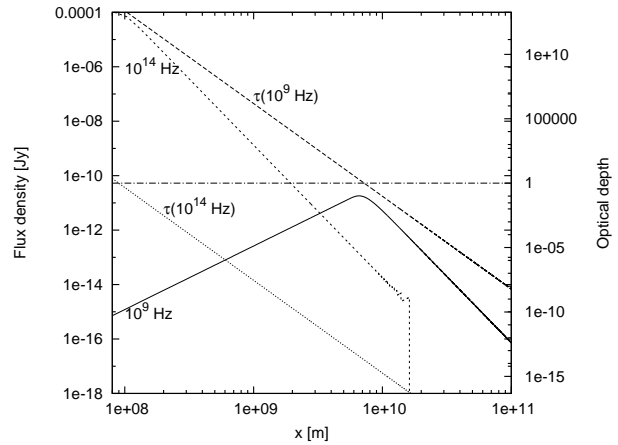


**Figure 5.** Emission from a single shell with adiabatic energy losses: radio and infra-red frequencies are shown. The shell optical depth,  $\tau_\nu$ , is also shown; the horizontal line marks optical depth of unity.

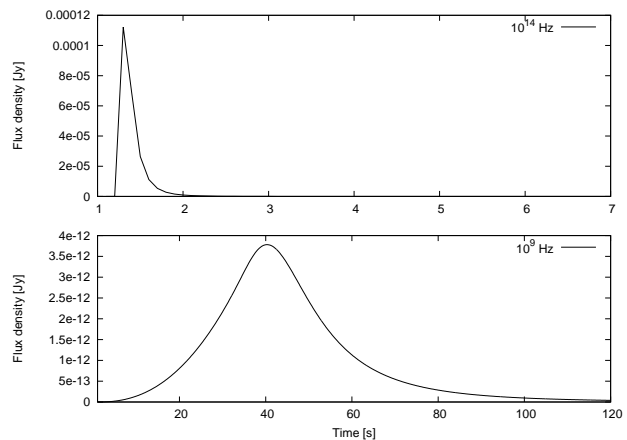


**Figure 6.** Infra-red and radio lightcurves for a single shell with adiabatic energy losses.

vious scenario, the shell thermal energy is again set to zero. Therefore any increase in the shell volume is purely due to the lateral expansion of the jet.

The radio and infra-red spectra from a single shell, with the adiabatic energy losses taken into account, are shown in figure 5. When compared with the spectra with no energy losses, figure 3, there are two main differences that become apparent: the radio peak is at much lower flux value, and at much smaller distance along the jet. The infra-red peak flux values, however, remain relatively unchanged; the peak occurs at smaller radii when compared to the no energy losses case. These differences can be explained when one looks at how the shell energy density changes with and without the energy losses present.

The shell optical depth is a function of the shell's energy density, i.e. a shell becomes optically thin to lower frequencies as the energy density drops. When energy losses are not considered, the change in the shell volume solely effects the change in the energy density. However, when the adiabatic energy losses are taken into account, the energy losses along with an increase in the shell volume drive the change

**Table 2.** The properties of the two shells injected in the double-ejection scenario shown in figures 7, 8, 9 and 10

Parameter	shell 1	shell 2
Inj. time	1 s	10 s
Mass	$1 \times 10^6$ kg	$1 \times 10^{10}$ kg
$\Gamma$	2.0	3.0
$dl$	$1 \times 10^5$ m	$1 \times 10^7$ m

in the shell energy density. In such a scenario, there is a two fold effect on the shell energy density: increase in the shell volume and the decrease in the shell internal energy. This then means that the shell optical depth, for a given frequency, changes more rapidly than when only the volume is effecting the change. The emission intensity, however, is also affected by the energy losses. With the adiabatic energy losses active a shell may be able to peak, for example, in radio frequencies at smaller jet radii,  $x$ , but the peak intensity is lower due to the energy losses suffered by the emitting electrons and the magnetic field. (If longitudinal expansion is also taken into account then the energy losses are accelerated and a shell is able to peak in radio frequencies even earlier with a further decrease in flux values). This can be seen in figure 5, and the lightcurves in figure 6, where the peak radio flux is nearly two orders of magnitude lower when compared with the peak radio flux in figure 3. The infra-red peak flux on the other hand suffers a relatively small reduction. This is due to the shell becoming optically thin to IR frequency very quickly in both cases, thus not having the time to suffer much energy energy losses. When the adiabatic losses are active, the shell starts off optically thin to IR. This is because the relative change in volume from the moment of injection to the subsequent time step being sufficient to drop the shell energy density below the limit for the shell becoming optically thin to infra-red frequencies. The initial volume of a shell, in addition to relative change in volume, also plays a part in how quickly that shell becomes optically thin to a given frequency: a large enough shell could start off as optically thin to infra-red frequencies. The sharp cut off for the infra-red flux, in figure 4, is due to  $\gamma_{max}$  dropping below the energy threshold for the power-law electrons to emit in the infra-red.

### 3.2 Double ejection

A double ejection scenario involves two shells being injected into the jet volume with a time interval,  $dt_{inj}$ , between them. If the second shell,  $j$ , has a higher velocity than the preceding shell,  $j-1$ , then the two shells should eventually collide. This scenario also demonstrates the core principle of multiple ejections: a large number of two-shell collisions taking place all along the jet to give rise to multiple shocks.

The shock-zone location, mentioned in the previous scenario, is set at zero. This means that the shells are injected with some internal energy instead of gaining it after passing through an arbitrary point. The adiabatic losses are also modelled, but only due to lateral expansion of the jet; the shell thermal energy is set to be zero.

The properties of the two shells injected into the jet volume are outlined in table 2. The first shell, ( $j-1$ ), is not

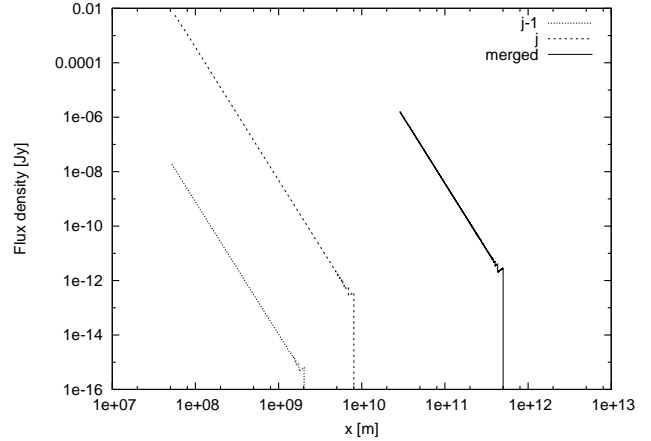


**Figure 7.** The infra-red ( $1 \times 10^{14}$  Hz) emission from the two injected shells that later on merge (at  $\sim 100$ s) to become a single shell. The properties of the two injected shells are outlined in table 2 while the simulation parameters are outlined in table 3. Adiabatic energy losses due to lateral expansion only are being modelled.

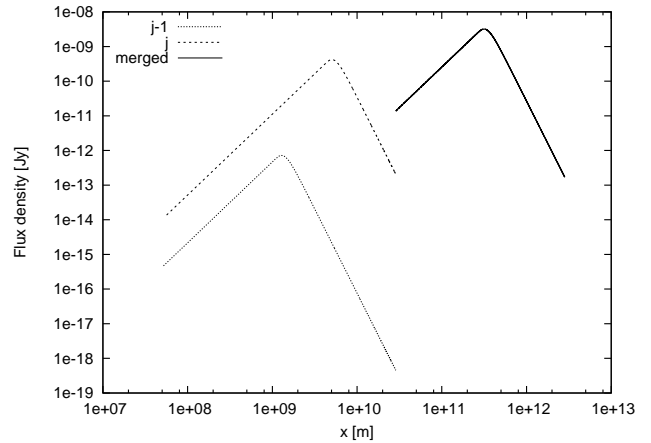


**Figure 8.** The radio ( $1 \times 10^9$  Hz) emission from the two shells injected that later on merge (at  $\sim 100$ s) to become a single shell. The properties of the two shells are outlined in table 2 while the simulation parameters are outlined in table 3. Adiabatic energy losses due to lateral expansion only are being modelled.

**Table 3.** The parameters used for double-ejection scenario.

Parameter	Figures 7, 8, 9 and 10
$\varphi$	$5^\circ$
$\theta$	$40^\circ$
$D$	2 kpc
$u_e$	0.5
$u_B$	0.5
$u_{th}$	0.0
$x_{shock}$	0.1 ls
$E_{frac}$	0.2
Sim. Duration	$1 \times 10^4$ s

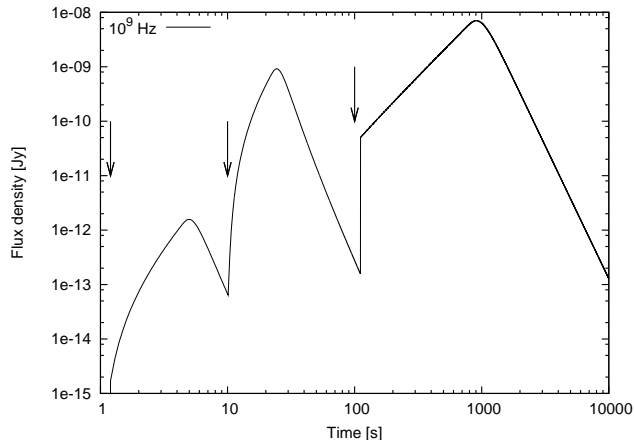


**Figure 9.** The lightcurve for the radio emission. The two arrows on the left signify injection of the two shells; the third arrow shows the time of merger. Initially (after the second shell injection at 10s) the lightcurve comprises emission from both the shells; later, after merger at  $\sim 100$ s, only a single shell exists in the jet. The properties of the two shells are outlined in table 2; the simulation parameters are outlined in table 3. The unusual  $\log(\text{time})$  is used for demonstrative purposes.

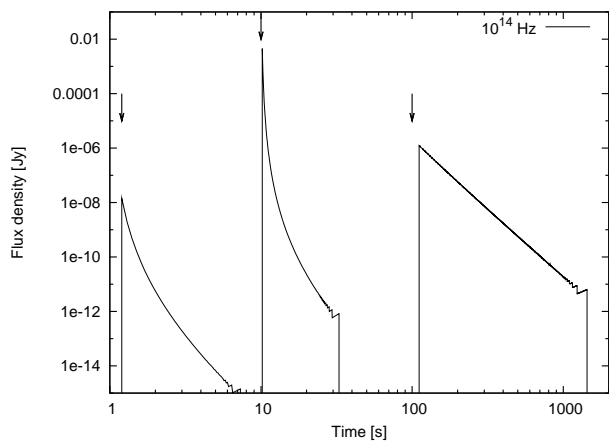


**Figure 10.** The lightcurve for the infra-red emission. The two arrows on the left signify injection of the two shells; the third arrow shows the time of merger. Initially (after the second shell injection at 10s) the lightcurve comprises emission from both the shells; later, after merger at  $\sim 100$ s, only a single shell exists in the jet. The properties of the two shells are outlined in table 2; the simulation parameters are outlined in table 3. The unusual  $\log(\text{time})$  is used for demonstrative purposes.

only less massive than the following one,  $j$ , but also larger. The combination of these parameters means that  $(j - 1)$  becomes optically thin to lower frequencies sooner than  $(j)$ . This can be seen in the figures 7 and 8 where the radio peak for shell  $(j - 1)$  is at much smaller jet radii than that for shell  $j$ ; in the case of IR emission, shell  $(j - 1)$  is already optically thin at those frequencies, when it is injected, while  $j$  reaches the peak IR flux later. The figures also show the point where the two-shell collision, or merger, takes place: it is marked by a sharp increase in both the radio and the IR emissions. The infra-red emission had in fact faded away completely

by the time the merger took place; thus, demonstrating the re-energization aspect of these collisions/internal shocks.

The lightcurves shown in figures 9 and 10 illustrate the lag between the high and the low frequency peaks, already seen from individual shells. In this case, however, the lightcurves show the total emission from the entire jet (only two shells for this scenario; multiple shells case is presented below). The radio emission not only lags behind the infra-red emission, but also has a much lower peak flux value (due to energy losses). Also, the radio emission rise and decay times are much longer than the infra-red times. In the case of infra-red, there is a sharp rise in the emission at the point of shell merger. As mentioned earlier, the infra-red fades away almost completely by the time the shell collision takes place. The merger, however, has a compression effect, thus increasing the energy density of the newly formed shell, causing it to start emitting in infra-red. The internal energy generated at the collision is still not sufficient to make the shell optically thick to infra-red; therefore, we do not see a slow rise in the infra-red flux from the merged shell. The picture is slightly different for the radio: the merged shell has high enough energy density that it becomes optically thick to the radio frequencies, leading to a slow rise in the flux. The other point to note, for the radio, is that after the second shell is injected into the jet, it takes a long time before the maximum flux is reached. This is due to the second shell taking a long time to become optically thin to the radio frequencies.

### 3.3 Multiple ejections

The multiple ejections set-up is also demonstrated with and without adiabatic energy losses taking place. When the energy losses are absent, the internal shocks/collision are also omitted as no energy replenishment is required; the collisions, however, are modelled when energy losses are incorporated. The shell properties in the case of collisions set-up are sampled from a *pseudo*-random distribution (as described in section 2.5).

#### 3.3.1 Without energy losses

If the time gap between ejection is small then an almost continuous jet can be approximated by multiple ejections. All the shells are injected with the same properties (time gap, velocity etc.), hence no collisions take place. The simulation parameters are given in table 4.

The spectrum shown in figure 11 shows how a flat spectrum (for a specific frequency range) can be recovered when no energy losses are considered. This set up can be compared to a situation where one assumes a constant replenishment of any energy losses by an unknown mechanism (Blandford & Königl 1979). The evolution of a radio and an IR frequency along the jet can be seen in figures 12 and 13 respectively. The two frequencies show a very different behaviour: IR spectrum shows a constant decline while the radio spectrum peaks much further down the jet. A look at the optical depths for the two frequencies shows that the injected shells, and ultimately the jet, is optically thin to infra-red ( $\tau_\nu \ll 1$ ); in the case of the radio frequency the jet becomes optically thin at a large distance from the source.



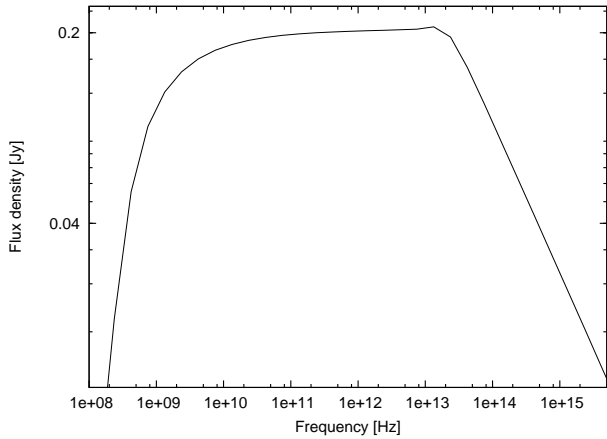


**Figure 11.** Spectrum of a jet modelled using multiple ejections (without energy losses). An almost flat spectrum is achieved over a large frequency range. It should be noted that the low frequency turn over point is dictated by the duration of the simulation: longer simulation means a longer jet which means a lower frequency turnover. (see table 4 for parameters).

**Table 4.** The parameters used to demonstrate multiple ejections (without energy losses).

Parameter	Figures 11, 12, 13, 14
$\varphi$	$5^\circ$
$\theta$	$40^\circ$
$D$	2 kpc
$L_W$	$1 \times 10^{30}$ J/s
$\Gamma$	2.0
$l_{scale}$	0.2
$u_e$	0.5
$u_B$	0.5
$u_{th}$	0.0
$x_{shock}$	0.0 ls
$E_{frac}$	0.01
$dt_{inj}$	$\sim 1$ s
Sim. Duration	$5 \times 10^4$ s

(The same behaviour was observed in the case of single ejections as well). The emission for a range of frequencies (radio  $< \nu <$  infra-red) are shown in figures 14. The different emissions shown in figure 14 follow the  $R_{\tau \approx 1} \propto \nu^{-1}$  relation (as predicted analytically by Blandford & Königl (1979)).

### 3.3.2 With adiabatic energy losses

The internal shocks are a possible way to address the problem of replenishing the energy losses in a jet. In the simulations presented below the shells are expanding both longitudinally and laterally; therefore the adiabatic losses can be extremely fast, making the flat spectrum difficult to obtain. The spectra from simulations where shells are not injected with any internal energy can be compared with the spectra from the simulation where shells are injected with internal energy: internal shocks are the only source of the internal energy production in the former case, whereas in the latter they serve to replenish the energy losses only.

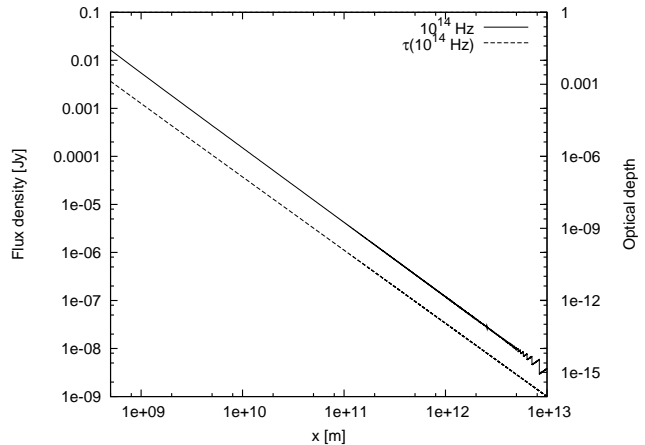


**Figure 12.** The infra-red emission of a multiple ejections jet (without energy losses). Optical depth corresponding to the infra-red frequency is also plotted (long dashed line). The wriggles at the end of the IR spectrum are a numerical artefact.(see table 4 for parameters).

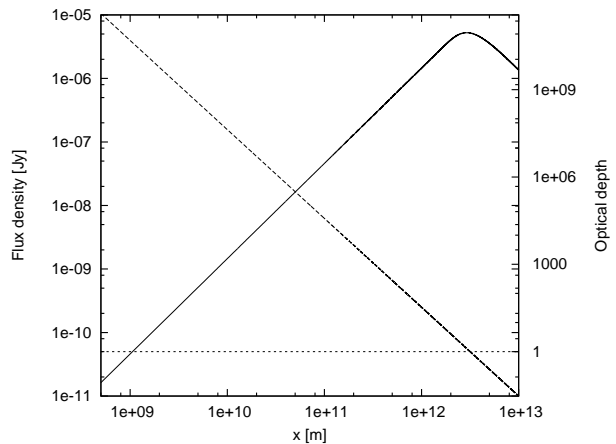


**Figure 13.** The radio emission of a multiple ejections jet (without energy losses). Optical depth corresponding to the radio frequency is also plotted (long dashed line); short dashed line shows where the optical depth  $\sim 1$ .(see table 4 for parameters).

The spectrum shown in figure 15 shows a highly inverted spectrum, when the shells are not injected with any internal energy. The internal shocks taking place are not sufficient to produce the internal energy in addition to replenish the energy losses that are taking place, resulting in an inverted spectrum.

On the other hand, the spectra given in figure 16 illustrate how it is possible to obtain an inverted/flat spectra even with adiabatic energy losses taking place. In order to achieve this, it is necessary to inject the shells with internal energy. In other words, when the internal shocks are used to produce the internal energy, plus replenish the adiabatic losses, a flat spectrum is not obtainable; however, when the internal shocks are used for energy replenishment only, the flat/inverted spectrum is recovered. It should be noted that the role played by the injected internal energy ( $E_{frac} > 0.0$ ) is somewhat more complicated as it also influences the longitudinal expansion rate of the shells, thus how

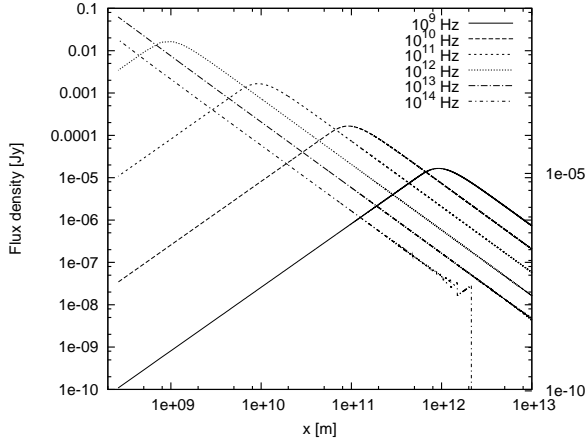


**Figure 14.** The emission as a function of the jet radius for a range of frequencies in a multiple ejections jet (without energy losses). (see table 4 for parameters).

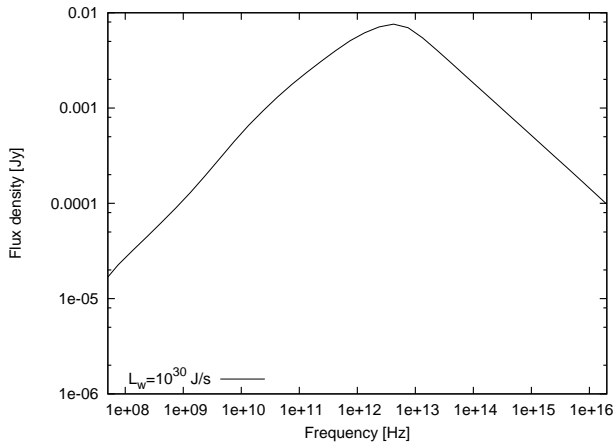


**Figure 15.** Time averaged spectrum ( $\sim 1ks$ ) from a multiple ejection jet with adiabatic energy losses. The shells involved undergo lateral and longitudinal expansion. The shells are not injected with any internal energy. (see table 5 for parameters).

**Table 5.** The parameters used for multiple ejections jet with adiabatic energy losses.

Parameter	fig 15	fig 16	fig 17
$\varphi$	$5^\circ$	$5^\circ$	$5^\circ$
$\theta$	$40^\circ$	$40^\circ$	$40^\circ$
$D$	2 kpc	2 kpc	2 kpc
$L_W$	$1 \times 10^{30}$ J/s	$1 \times 10^{28-30}$ J/s	$1 \times 10^{30}$ J/s
$\Gamma_{min}$	1.5	1.5	2.0
$\Gamma_{max}$	2.0	2.0	2.0
$l_{scale}$	0.2	0.2	0.2
$u_e$	0.33	0.33	0.5
$u_B$	0.33	0.33	0.5
$u_{th}$	0.33	0.33	0.0
$E_{frac}$	0.0	0.01	0.01
$dt_{inj}$	$\sim 1$ s	$\sim 1$ s	$\sim 1$ s
Sim. Duration	$5 \times 10^4$ s	$5 \times 10^4$ s	$5 \times 10^4$ s

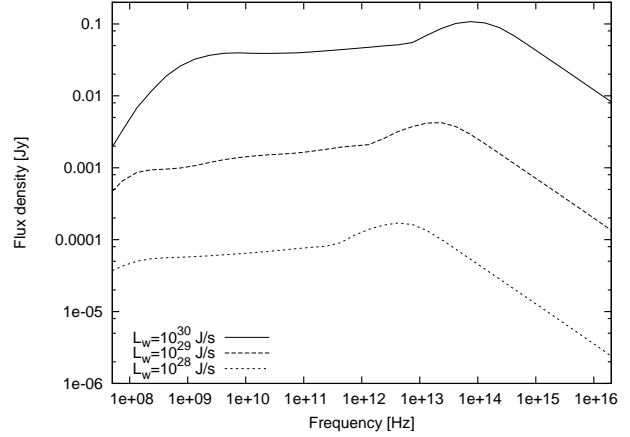


**Figure 16.** Time averaged inverted/flat spectra ( $\sim 2ks$ ) from multiple ejection jets with the adiabatic energy losses. The three spectra correspond to different jet kinetic luminosities. The shells involved undergo lateral and longitudinal expansion. The shells are injected with internal energy, creating a much different spectrum from seen in figure 15.(see table 5 for parameters).

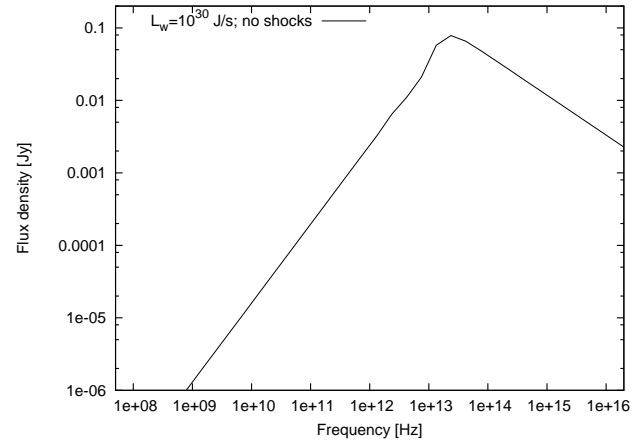


**Figure 17.** Time averaged inverted spectrum ( $\sim 2ks$ ) from multiple ejection jets with the adiabatic energy losses. The adiabatic energy losses are due to the lateral expansion of the shells. See table 5 for parameters.

quickly a shell becomes optically thin to different frequencies. When a shell is not injected with any internal energy ( $E_{frac} = 0.0$ ), the longitudinal expansion does not begin until after the first merger; this means the colliding shells are quite small, causing higher frequencies to dominate the spectrum. Figure 17 shows a highly inverted spectrum for a jet where the shells are injected with some internal energy, but no shocks/mergers are taking place; the adiabatic energy losses are also being modelled (this is an almost identical scenario to the one shown in figure 11, except for the additional adiabatic energy losses here). It is clear that both the internal energy and the shocks re-acceleration are necessary to achieve a flat/inverted spectrum whilst taking the adiabatic energy losses into account.

We can also note in figure 16 that the flux is correlated with the jet kinetic luminosity. This is because  $E_{frac}$  is scaled according to the relativistic energy of the shell,

which is related to the mass and the bulk Lorentz factor of the shell; the mass is dependent on the kinetic luminosity (see equation 24), which ultimately means that the higher jet kinetic luminosity creates shells with higher internal energy, thus producing greater flux. Higher energy density also means that a shell would be optically thick to higher frequencies. The effects of jet kinetic luminosity on the flux (and the spectrum) are degenerate with  $E_{frac}$  parameter: a lower luminosity jet, but with the higher  $E_{frac}$  value can produce similar results. This degeneracy extends to any parameter that influences the internal energy of the shell at injection; for instance, the jet opening angle and the shell length ( $l_{scale}$ ) will also influence the form of spectra obtained. The spectra show in figure 16 conform approximately to the relation:  $F_\nu \propto L_W^{1.4}$ . This is in agreement with the relation found analytically by Heinz & Sunyaev (2003), stating:  $F_\nu \propto L_W^{1.4}$ .

The flat/inverted spectra produced have shown other interesting correlations: both the high and the low frequency turnover points in the spectrum correspond to certain jet properties. In the case of the high frequency break, the higher the jet power (mainly  $L_W$ , but also  $E_{frac}$ ), the higher the break frequency. The high frequency break scales approximately as:  $\nu_b \propto L_W^{0.6}$ , which is remarkably close to previously observed and calculated relation of  $\nu_b \propto L_W^{0.7}$  (Falcke & Biermann 1995; Markoff et al. 2003; Heinz & Sunyaev 2003). The low frequency turnover, on the other hand, is also affected by the jet luminosity, but the re-energization by the internal shocks appears to play the biggest role: both the number of shells present in the jet and the collision radii of the shells influence the low frequency turnover.

## 4 CONCLUSIONS

The results presented in this paper show how it is possible to reproduce a canonical flat spectrum even when a discretized jet is used. We have also shown how flat/inverted spectrum is also reproducible if the internal shocks are used for energy replenishment. If the internal shocks are used for the initial electron acceleration, on top of replenishing the energy losses, the spectra become highly inverted ( $\alpha > 0$ ).

The multiple internal shocks created by multiple ejection into the jet volume can provide a considerable amount of energy to the shells. The results show that even with an essentially random distribution of shells velocities and injection times, adequate re-energization is possible: the flat/inverted spectrum is achieved. This is an important result in furthering our understanding of the jet physics. We have also seen that the high frequency break in flat/inverted spectra is correlated with the jet power; the lower frequency turnover shows dependence on the number of shells present in the jet in addition to their collision radii. Further investigation is required to quantify fully the relation that may exist between the jet properties and various break frequencies. However, the break frequency correlations seen thus far, are in agreement with the theoretical prediction as well as the observations.

The results outlined above also hint at being able to tie the timing properties (X-ray to Infra-red in the case of X-ray binaries) with the jet physics. It should also be possible to

link the shell properties (such as time gap between ejections and the bulk Lorentz factor) with X-ray timing information for example. Using the X-ray lightcurves to drive such jets, we can then look at the infra-red lightcurves produced, we have an additional diagnostics for checking self consistency in the model. This investigation may also show how a “single blob” picture may arise, where the radio rise and decay times (plus the flux) are very similar to the ones for the infra-red (Mirabel et al. 1998; Fender & Pooley 2000). This is clearly not compatible with the single shell picture presented in this paper. It can then be assumed that it is not a simple scenario like a single large blob being responsible for the observed massive ejection events. We must therefore delve further to try and understand why this is currently not reproducible with our model.

It is safe to conclude that the results presented in this paper do not exclude other re-acceleration models, but the internal shocks model holds much promise in being able to reproduce the often seen flat/inverted spectra in addition to opening up the avenue for studying jet timing properties.

## ACKNOWLEDGMENTS

The authors are grateful to the anonymous reviewer for many helpful comments. OJ is grateful to STFC for the Ph.D. funding. OJ would also like to thank Phil Uttley for the insightful discussion and reading the paper. OJ is also grateful to Tom Maccarone, Tony Bird, Clément Cabanac, Piergiorgio Casella and Georgi Pavloski for many useful discussions.

## APPENDIX A: THE CODE

We are in principle open and receptive to others wishing (in collaboration) to utilize our code to model and test different jet scenarios. If you are interested, please contact the author.

The following section outlines all the customizable parameters in our model. With efficiency and expandability in mind, the model is coded in C++. Effort has been made to minimize dependencies and use GNU software only. Once compiled, the code can read in all the parameters from a simulation parameters file and a shell parameters file; for any subsequent changes to the parameters, the code does not require re-compilation.

The customizable parameters for the code are as follows:

**Jet Luminosity:** Used when shell properties are *pseudo*-random. This determines the shell mass based on how many shells need to be injected. [J/s]

**BLF\_max:** Used when shell properties are *pseudo*-random. This sets the mean of a Gaussian distribution to be sampled from. [ $\Gamma_{max}$ ]

**BLF\_min:** Used when shell properties are *pseudo*-random. This sets the mean of a Gaussian distribution to be sampled from. [ $\Gamma_{min}$ ]

**shell\_width\_factor:** Sets the initial shell size, along the jet axis using the relation outlined in equation 25. [no units]

**jet\_opening\_angle:** The full opening angle of the jet. [degrees]

**source\_distance:** Distance to the source being modelled. [kpc]

**EThermal\_frac:** The fraction of the shell internal energy to be given to the thermal energy; causes the longitudinal expansion. [no units]

**EelecKin\_frac:** The fraction of the shell internal energy to be given to the total electron kinetic energy; determines the power-law distribution parameters. [no units]

**EMagnet\_frac:** The fraction of the shell internal energy to be given to the magnetic energy; affects the magnetic field strength. [no units]

**powerlaw\_index:** The power-law index,  $p$ , of the electron power-law distribution. [no units]

**e\_gamma\_min:**  $\gamma_{min}$  of the power-law electrons. [ $\gamma$ ]

**e\_gamma\_max:**  $\gamma_{max}$  of the power-law electrons. [ $\gamma$ ]

**nu\_min:**  $\nu_{min}$  for the frequencies being modelled; used when logarithmically spaced frequency range is used. [Hz]

**nu\_max:**  $\nu_{max}$  for the frequencies being modelled; used when logarithmically spaced frequency range is used. [Hz]

**nu\_points:** Determines the number of points for the logarithmic frequency grid. [no units]

**individual\_frequencies** Switch to turn on logarithmically spaced frequency range; takes min. and max from above. [take integer values: n=off (then uses two frequencies below; y=on)]

**nu\_1** Used if only two frequencies being sampled. [Hz]

**nu\_2** Used if only two frequencies being sampled. [Hz]

**increase\_time\_resolution** A switch for increasing sampling, for radiative emission, of the jet at the time interval given below. [takes integer values: n=off (in this case the jet is sampled only at “events”; y=on)]

**step\_resolution** If the above switch is on, this determines the sampling time interval. [s]

**total\_run\_duration** Total run time of the simulation. [s]

**shell\_inj\_duration** The length of time for the shells injection. [s]

**avg\_ejection\_gap** Sets the mean of the Gaussian distribution for sampling the time interval between shell injections. [s]

**use\_shell\_file** A switch for reading a file with shell properties: injection time, shell mass, shell Lorentz factor, shell width. [takes integer values: n=off; y=on (when on, jet\_luminosity, BLF\_max, shell\_width, shell\_inj\_duration, and avg\_ejection\_gap are all deactivated)]

**shell\_file** Name of the file with shell parameters. [should contain 4 columns with the corresponding shell properties:injection time, shell mass, shell Lorentz factor, shell width.]

**write\_results\_file** A switch to activate writing every time step to a file. [takes integer values: n=off; y=on]

**results\_file** Name of the file for the above switch.

**final\_time\_step** A switch to activate writing final time step of the simulation. [takes integer values: n=off; y=on]

**lightcurve\_file** Name of the file for writing the light curve data. [Always written by default]

**in\_vacuum\_expansion** A switch to deactivate adiabatic losses.

**inj\_int\_energy** A switch to inject the shells with internal energy, after they have passed the “shock location”.

**rel\_mass\_frac** Scale the amount of internal energy given to the shell by a fraction of the of the shell’s relativistic energy.

**shock\_location** The shock location. Used when injecting with internal energy. [light seconds]

**slow\_energization** A switch to activate slow energization; the shells are not energized instantly, but given the energy over a length of time determined by the shock crossing time. [takes integer values: n=off, y=on]

## REFERENCES

- Blandford R. D., Königl A., 1979, The Astrophysical Journal, 232, 34  
 Cawthorne T. V., 1991, Interpretation of parsec scale jets. pp 187–+  
 Corbel S., Fender R. P., 2002, The Astrophysical Journal, 573, L35  
 Falcke H., 1996, The Astrophysical Journal Letters, 464, L67+  
 Falcke H., Biermann P. L., 1995, Astronomy and Astrophysics, 293, 665  
 Falcke H., Markoff S., 2000, Astronomy and Astrophysics, 362, 113  
 Fender R. P., 2001, Mon. Not. R. Astron. Soc., 322, 31

- Fender R. P., Belloni T. M., Gallo E., 2004, *Mon. Not. R. Astron. Soc.*, 355, 1105
- Fender R. P., Pooley G. G., 2000, *Mon. Not. R. Astron. Soc.*, 318, L1
- Heinz S., Begelman M. C., 2000, *The Astrophysical Journal*, 535, 104
- Heinz S., Sunyaev R. A., 2003, *Mon. Not. R. Astron. Soc.*, 343, L59
- Hjellming R. M., Johnston K. J., 1988, *The Astrophysical Journal*, 328, 600
- Kaiser C. R., 2006, *Mon. Not. R. Astron. Soc.*, 367, 1083
- Longair M. S., 1994, *High energy astrophysics. Vol.2: Stars, the galaxy and the interstellar medium*. Cambridge: Cambridge University Press, —c1994, 2nd ed.
- Markoff S., Falcke H., Fender R., 2001, *Astronomy and Astrophysics*, 372, L25
- Markoff S., Nowak M., Corbel S., Fender R., Falcke H., 2003, *Astronomy and Astrophysics*, 397, 645
- Marscher A. P., 1980, *The Astrophysical Journal*, 235, 386
- Mirabel I. F., Dhawan V., Chaty S., Rodriguez L. F., Marti J., Robinson C. R., Swank J., Geballe T., 1998, *Astronomy and Astrophysics*, 330, L9
- Panaitescu A., Mészáros P., 1999, *The Astrophysical Journal*, 526, 707
- Pe'er A., Casella P., 2009, *ArXiv e-prints* 0902.2892
- Spada M., Ghisellini G., Lazzati D., Celotti A., 2001, *Mon. Not. R. Astron. Soc.*, 325, 1559